



NRL/MR/7320--15-9611

NFLUX PRE: Validation of New Specific Humidity, Surface Air Temperature, and Wind Speed Algorithms for Ascending/Descending Directions and Clear or Cloudy Conditions

NEIL VAN DE VOORDE

Vencore

Services and Solutions Group

Stennis Space Center, Mississippi

JACKIE MAY

CLARK ROWLEY

Ocean Dynamics and Prediction Branch

Oceanography Division

June 18, 2015

Approved for public release; distribution is unlimited.

REPORT DOCUMENTATION PAGE

Form Approved
OMB No. 0704-0188

Public reporting burden for this collection of information is estimated to average 1 hour per response, including the time for reviewing instructions, searching existing data sources, gathering and maintaining the data needed, and completing and reviewing this collection of information. Send comments regarding this burden estimate or any other aspect of this collection of information, including suggestions for reducing this burden to Department of Defense, Washington Headquarters Services, Directorate for Information Operations and Reports (0704-0188), 1215 Jefferson Davis Highway, Suite 1204, Arlington, VA 22202-4302. Respondents should be aware that notwithstanding any other provision of law, no person shall be subject to any penalty for failing to comply with a collection of information if it does not display a currently valid OMB control number. **PLEASE DO NOT RETURN YOUR FORM TO THE ABOVE ADDRESS.**

1. REPORT DATE (DD-MM-YYYY) 18-06-2015		2. REPORT TYPE Memorandum Report		3. DATES COVERED (From - To)	
4. TITLE AND SUBTITLE NFLUX PRE: Validation of New Specific Humidity, Surface Air Temperature, and Wind Speed Algorithms for Ascending/Descending Directions and Clear or Cloudy Conditions				5a. CONTRACT NUMBER	
				5b. GRANT NUMBER	
				5c. PROGRAM ELEMENT NUMBER 0602435N	
6. AUTHOR(S) Neil Van de Voorde,* Jackie May, and Clark Rowley				5d. PROJECT NUMBER	
				5e. TASK NUMBER	
				5f. WORK UNIT NUMBER 73-6764-05-5	
7. PERFORMING ORGANIZATION NAME(S) AND ADDRESS(ES) Naval Research Laboratory Oceanography Division Stennis Space Center, MS 39529-5004				8. PERFORMING ORGANIZATION REPORT NUMBER NRL/MR/7320--15-9611	
9. SPONSORING / MONITORING AGENCY NAME(S) AND ADDRESS(ES) Office of Naval Research One Liberty Center 875 North Randolph Street, Suite 1425 Arlington, VA 22203-1995				10. SPONSOR / MONITOR'S ACRONYM(S) ONR	
				11. SPONSOR / MONITOR'S REPORT NUMBER(S)	
12. DISTRIBUTION / AVAILABILITY STATEMENT Approved for public release; distribution is unlimited.					
13. SUPPLEMENTARY NOTES *Vencore, Services and Solutions Group, Stennis Space Center, MS					
14. ABSTRACT The Naval Research Laboratory (NRL) Ocean Surface Flux System (NFLUX) has been updated to include additional satellite sensors and improved satellite retrieval algorithms. In addition to data from the Special Sensor Microwave Imager/Sounder (SSMIS) and the Advanced Microwave Sounding Unit (AMSU) sensors, NFLUX also processes data from the Advanced Technology Microwave Sounder (ATMS) and Advanced Microwave Scanning Radiometer-2 (AMSR2) sensors. The original multiple linear regression algorithms have been updated to multiple polynomial regression algorithms based on a hyperbolic function, which also eliminates the need for additional adjustments for observations in the higher ranges of the products. For each satellite and ocean surface product combination four separate algorithms were developed based on ascending/descending orbits as well as clear/cloudy conditions. Global statistics are presented for each of the algorithm types for each sensor.					
15. SUBJECT TERMS SSMIS AMSR2 Wind speed AMSU Air temperature ATMS Specific humidity					
16. SECURITY CLASSIFICATION OF:			17. LIMITATION OF ABSTRACT Unclassified Unlimited	18. NUMBER OF PAGES 30	19a. NAME OF RESPONSIBLE PERSON Jackie May
a. REPORT Unclassified Unlimited	b. ABSTRACT Unclassified Unlimited	c. THIS PAGE Unclassified Unlimited			19b. TELEPHONE NUMBER (include area code) (228) 688-4302

Table of Contents

1. Scope.....	1
2. SNPP Advanced Technology Microwave Sounder.....	2
2.1 Algorithm Basis	2
2.2 Rain Flags	3
2.3 Clear/Cloudy	3
2.4 ATMS Performance	4
3. GCOM-Water 1 Advanced Microwave Scanning Radiometer-2 Sensor.....	7
3.1 JAXA Level-1R Data	7
3.2 Rain Flagging of Data	8
3.3 Clear/Cloudy	8
3.4 AMSR2 Performance	9
4. SSMIS Update	14
4.1 Rain Flagging and Clear/Cloudy SSMIS.....	15
4.2 SSMIS Performance.....	15
5. AMSU Update.....	18
5.1 AMSU Performance	20
6. Summary and Discussion.....	21
7. References.....	24
8. Acronyms and Abbreviations.....	25

List of Figures

Figure 1: Example microwave response	3
Figure 2: ATMS and NAVGEM QA performance	5
Figure 3: ATMS and NAVGEM QA global bias	5
Figure 4: ATMS and NAVGEM TA performance	6
Figure 5: ATMS and NAVGEM TA global bias	7
Figure 6: AMSR2 performance	9
Figure 7: NAVGEM performance	9
Figure 8: AMSR2 QA global value probability	11
Figure 9: Two-dimensional probability distribution of air temperature bias	12
Figure 10: AMSR2 TA global value probability	12
Figure 11: Two-dimensional probability distribution of wind speed bias	13
Figure 12: Probability distribution of lower wind speeds as a function of the in situ wind speed	14
Figure 13: Probability distribution for higher wind speeds	14
Figure 14: Mean wind speed compared to buoy winds	23

List of Tables

Table 1: NFLUX observational inputs	1
Table 2: ATMS and AMSU frequencies.....	2
Table 3: ATMS specific humidity global performance	4
Table 4: Related NFLUX product performance.....	4
Table 5: ATMS air temperature global performance.....	6
Table 6: GCOMW1 AMSR2 channels.....	7
Table 7: AMSR2 algorithm performance.....	10
Table 8: AMSR2 and NAVGEM performance summary.....	10
Table 9: Match up metrics for QA bands.....	11
Table 10: Match up metrics for TA high values.....	13
Table 11: Performance metrics for wind speeds greater than 10 ms^{-1}	13
Table 12: SSMIS air temperature algorithm performance	15
Table 13: SSMIS specific humidity algorithm performance	16
Table 14: SSMIS wind speed algorithm performance	17
Table 15: SSMIS and NAVGEM performance summary.....	18
Table 16: POES AMSU algorithm performance.....	19
Table 17: Metop AMSU algorithm performance	20
Table 18: AMSU and NAVGEM performance summary	21
Table 19: Comparison of older algorithm performance with newer algorithms.....	22

1. Scope

The NFLUX PRE Validation Test Report (VTR, Van de Voorde et al., 2014) documented the initial capabilities and performance of the satellite retrieval component of the Naval Research Laboratory Ocean Surface Flux (NFLUX) system. This report provides additional information for: (1) new sensors, (2) changes in algorithm construction, and (3) expansion of the Defense Meteorological Satellite Program (DMSP) Special Sensor Microwave Imager/Sounder (SSMIS) sensor processing to retrieve surface air temperature (TA). Table 1 shows the updated suite of observations provided by the NFLUX system. This report documents the addition of the Suomi National Polar-orbiting Partnership (SNPP) Advanced Technology Microwave Sounder (ATMS) sensor and the Japanese Aerospace Exploration Agency (JAXA) Global Change Observation Mission-W1 (GCOM-W1) Advanced Microwave Scanning Radiometer-2 (AMSR-2).

Table 1: NFLUX observational inputs. The Naval Research Laboratory Ocean Surface Flux (NFLUX) system uses a combination of level 1B Sensor Data Record (SDR) satellite data, Environmental Data Record (EDR) readers, and direct observations (X) from buoys and ships to provide ocean surface state variables of specific humidity (QA), scalar wind speed (U10), and air temperature (TA). Local equatorial-crossing times of the ascending node (LTAN) are noted.

Platform / Sensor	QA	U10	TA	LTAN
DMSP F16 / SSMIS	SDR	SDR	SDR	17:22
DMSP F17 / SSMIS	SDR	SDR	SDR	17:49
DMSP F18 / SSMIS	SDR	SDR	SDR	17:06
POES N15 / AMSU	SDR		SDR	16:51
POES N18 / AMSU	SDR		SDR	15:23
POES N19 / AMSU	SDR		SDR	13:39
Metop-A / AMSU	SDR		SDR	21:29
Metop-B / AMSU	SDR		SDR	21:31
SNPP / ATMS	SDR		SDR	13:30
GCOMW1 / AMSR2	SDR	SDR	SDR	13:30
Metop-A / ASCAT		EDR		21:29
Metop-B / ASCAT		EDR		21:31
Oceansat2 / OSCAT		EDR		12:00
Coriolis / WindSat		EDR		18:00
Ships	X	X	X	n/a
Buoys	X	X	X	n/a

Algorithm updates include those for TA, specific humidity (QA), and surface wind speed (U10) for the Advanced Microwave Sounding Unit (AMSU) flying onboard the National Oceanographic and Atmospheric Administration Polar-orbiting Environmental Satellite (POES) and the European Organization for the Exploitation of Meteorological Satellites Metop satellites, as well as for QA and U10 for the SSMIS flying onboard the DSMP satellites. The basis algorithm used has been updated from multiple linear

regression to a multiple polynomial regression based upon a hyperbolic function described in section 2.1. In addition to the new algorithm basis, satellite orbital direction and an initial atmospheric condition were incorporated into the NFLUX system. Separate algorithms were developed for a matrix of ascending/descending orbits as well as clear or cloudy conditions.

2. SNPP Advanced Technology Microwave Sounder

The ATMS flies onboard the SNPP spacecraft. It is similar in terms of cross-track scanning and frequencies to the heritage AMSU instruments flying onboard the POES and Metop platforms. Table 2 shows a channel-by-channel comparison between the two sensors. For the AMSU and the ATMS sensors, the largest contribution to the surface state variables comes from the 53.6 GHz channel, based upon the magnitude of the coefficients in the algorithms. For AMSU, the second largest contributor is the 52.8 GHz channel. For ATMS, the 51.76 GHz channel is very similar in response to the 52.8 GHz channel. The 53.6, 52.8, and 51.76 GHz channels have peak vertical responses near 750, 850, and 950 hPa, respectively (Weng et al., 2012).

Table 2: ATMS and AMSU frequencies. Comparison between sensor frequencies used by ATMS and AMSU onboard the SNPP and POES satellites. The AMSU sensors onboard Metop A and B are the same as those onboard the POES. Values are shown in GHz.

ATMS	AMSU
23.8	23.8
31.4	31.399
50.3	50.299
51.76	---
52.8	52.8
53.6	53.6
88.2	89.0

2.1 Algorithm Basis

The original algorithms used in the NFLUX system applied a multiple linear regression. The coefficients were developed using a multi-resampling selection technique to subsample the large database of brightness temperatures and in situ observations in order to estimate the most probable coefficients for the linear model. In the initial development, we determined that an additional term gave a better prediction at the extreme values of QA, where the overall response of the sensor was no longer linear. Based on further examination of the response of the sensors channels to QA, shown in Figure 1, a new basis algorithm was selected to replace the linear algorithm. There is a highly linear response over the majority of the range; however, at the high end and to a lesser extent the lower end, the relationship between sensor response and QA is nonlinear. Figure 1 indicates the localized peaks (the blue dots) in the QA distribution with relation to the 31.4 GHz brightness temperature. The “S” shape indicated by the blue dots in the left panel is similar to a hyperbolic tangent function, shown in the right panel. New algorithms for QA, TA, and U10 using a multiple polynomial regression

(four-term, fifth-order) were inspired by the series expansion of the sinh and tanh functions. The new basis function also eliminates the need for the high QA value adjustment. The coefficients were developed based on match up data from January 2013 to mid-January 2014.

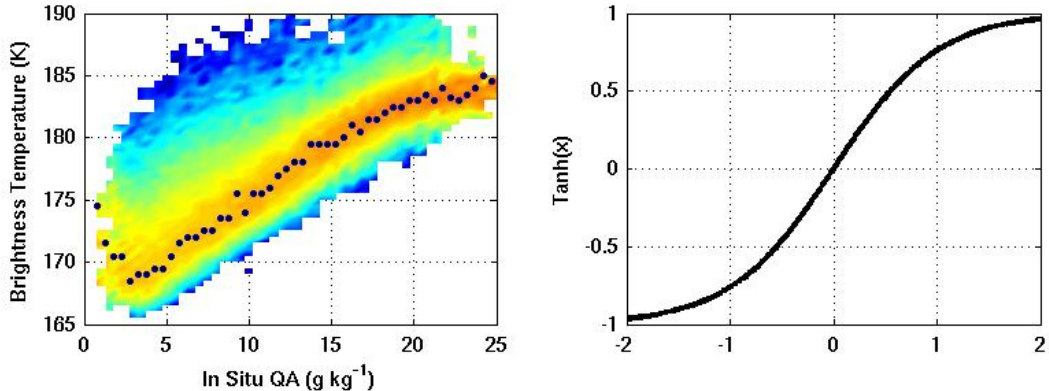


Figure 1: Example microwave response. The left panel shows the QA distribution with relation to the 31.4 GHz brightness temperature (the dots indicate trace mode values). The shape of the response is similar to a hyperbolic tangent (tanh) function shown in the right panel.

A suite of algorithms was developed to apply to ascending/descending orbital directions and clear/cloudy conditions. It is common in the relevant literature to separate the results for ascending or descending orbits (e.g., Roberts, et al., 2010 and John et al., 2013). The time difference of observation is essentially 12 hours between the ascending and descending, so that observations taken during the ascending orbit view the surface under different diurnal conditions than the descending orbit. Based on recent literature (e.g., Roberts et al., 2010), the state of the atmosphere was determined to be in either clear or cloudy based on a calculation of cloud liquid water path (LWP, the sum of the cloud liquid water and rainwater paths, or the vertically integrated liquid water content of the atmosphere).

2.2 Rain Flags

The ATMS rain flags are based on the AMSU rain flags (Hu et al., 2006). They were discussed in section 2.1.2 of Van de Voorde et al. (2014). The only difference in the two applications is the use of the 88.2 GHz channel in place of the 89.0 GHz channel of AMSU, without modification to the algorithm. Observations contaminated by rain are removed from processing in the data quality control component of the NFLUX system.

2.3 Clear/Cloudy

The methods of Weng and Grody (1994) and Grody et al. (2001) are used to estimate the LWP. Roberts et al. (2010) utilized a threshold of 0.025 mm water to distinguish clear and cloudy states, and that value was adopted for the NFLUX system. The ATMS LWP implementation utilizes the 23.8 and 31.4 GHz brightness temperatures and a view angle

based on the scan position of the sensor. The coefficients for the LWP calculation are taken from Equation 7 of Grody et al. (2001).

2.4 ATMS Performance

The performance metrics of the ATMS sensor for QA, shown in Table 3, can be compared with the original metrics for the AMSU sensors in Table 4 from Van de Voorde et al. (2014). While these two reports use different time periods, the AMSU and ATMS sensors are essentially equivalent, with the exception of the added channel on the ATMS. The ATMS QA product uses the new polynomial basis for the algorithms. The high-value adjustment factors detailed in equations 5 and 6 of the original VTR are no longer needed. The bias, or mean error (ME), for each ATMS product shows a significant improvement over the previous products that utilized multiple linear regression for the algorithm basis. The “cost” of the improvement in bias performance is a higher standard deviation (SD) and root mean square error (RMSE). A comparison to the Navy Global Environmental Model (NAVGEM) is shown. The match up dataset includes data from 01 Jan 2013 through 11 Jan 2014. NAVGEM v1.1 runs through 00Z 06 Nov 2013, and v1.2 runs from 12Z 06 Nov 2013 forward. Shown for ATMS and NAVGEM are ranges for the ME, RMSE and the correlation coefficient (R^2) for the 99% confidence limit (CL). ATMS is superior for ME for both products. For RMSE and R^2 , there is no statistically significant difference.

Table 3: ATMS specific humidity global performance. The global performance of the algorithms is compared to the atmospheric model performance. Units are in g water per kg dry air. Comparisons are based on match up data from 01 Jan 2013 through 11 Jan 2014 and contain 116110 observations. The combined results show the 99% CL low and high ranges.

	ME	SD	RMSE	R^2
Ascend - Clear	0.269	1.57	1.59	0.952
Ascend - Cloudy	-0.088	1.20	1.21	0.966
Descend - Clear	0.190	1.49	1.50	0.952
Descend - Cloudy	-0.151	1.18	1.19	0.963
Combined				
ATMS	0.84/0.22	--	1.41/1.54	0.96/0.97
NAVGEM	-0.67/-0.55	--	1.35/1.50	0.97/0.97

Table 4: Related NFLUX product performance. These results are based on matchups with in situ observations from January 2010 to December 2011. From Van de Voorde et al. (2014).

	ME	RMSE	R^2	Units
AMSU QA	-0.3307	1.6194	0.907	g kg^{-1}
AMSU TA	-0.2542	1.659	0.957	$^{\circ}\text{C}$
SSMIS QA	-0.2183	2.049	0.859	g kg^{-1}
SSMIS U10	0.6234	2.825	0.430	ms^{-1}
WindSat U10	0.7196	2.499	0.508	ms^{-1}

The impact of the differences between the ATMS QA product and NAVGEM is demonstrated in Figures 2 and 3. There is a clear divergence in the NAVGEM performance near 17 g kg^{-1} specific humidity shown in the right panel of Figure 2. The match up dataset between 17.5 and 22 g kg^{-1} includes 23.9% of all of the in situ data. Therefore the performance of either NAVGEM or NFLUX at high QA values will be an issue approximately a quarter of the time. For the entire range of QA, at the 99% CL, the RMSE for ATMS QA is between 1.17 to 1.23 g kg^{-1} , while NAVGEM is statistically worse, with a range of 1.27 to 1.34 g kg^{-1} . The left panel of Figure 3 shows the probability distribution (PD) and the right side shows the cumulative probability distribution (CPD) of the bias. The ATMS QA retrievals are more evenly distributed around the actual in situ values, while the NAVGEM values have a significant probability of being low approximately 75% of the time. Our prediction is that the latent heat flux, which is a function of wind speed and humidity, will be consistently high based on NAVGEM inputs, but less biased using the ATMS QA product.

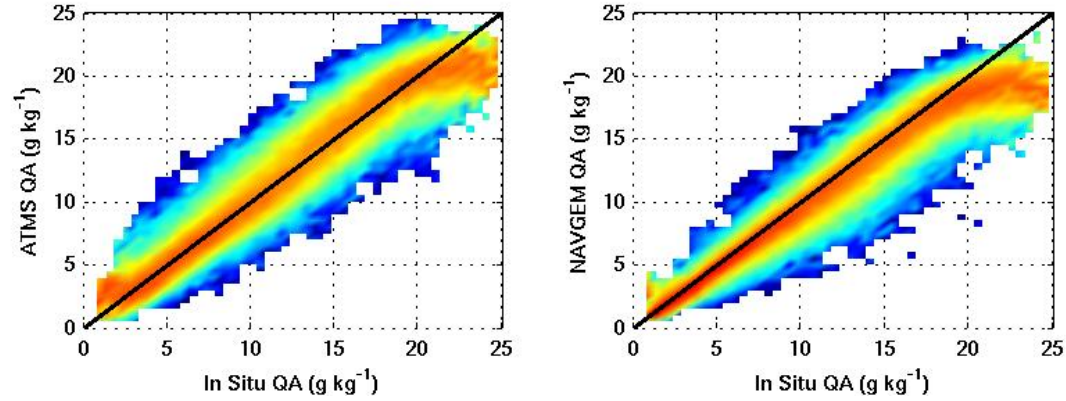


Figure 2: ATMS and NAVGEM QA performance. The overall performance is shown. The distribution shows normalized binned probability distributions throughout the entire range of data. The distribution is color-coded where warmer colors indicate bins with higher observation populations. The ATMS QA product shows improved bias over the atmospheric model.

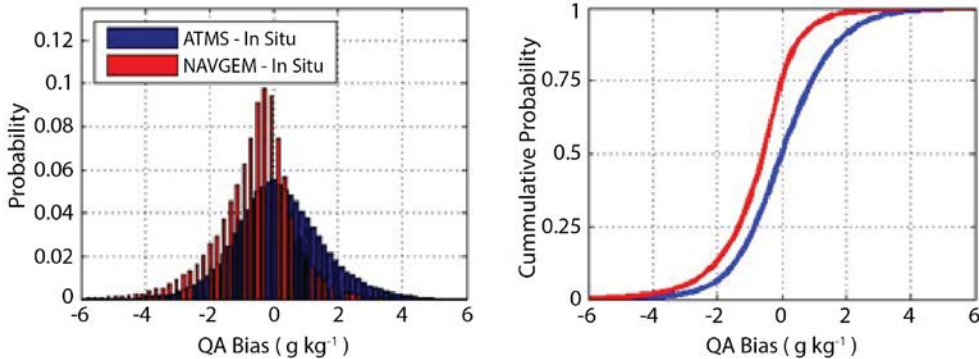


Figure 3: ATMS and NAVGEM QA global bias. The difference in the global performance between the ATMS QA product and the NAVGEM data set is shown. NAVGEM shows a clear negative bias, but with a lower standard deviation than the ATMS product in the left panel. The cumulative probability of the observation bias is shown on the right panel. The ATMS retrievals show a much more uniform distribution of errors than the atmospheric model.

The performance metrics of the ATMS sensor for TA using the new polynomial basis for the algorithms, shown in Table 5, can be compared with the original metrics for the AMSU sensors in Table 4. The surface TA for ATMS and its comparison with the performance of the NAVGEM is shown in Figure 4. As with the ATMS QA performance shown in Figure 2, the ATMS algorithm extreme range performance is improved when compared to the NAVGEM data. The model values are based on the tau 0 fields from the 0Z or 12Z model runs within the local NAVGEM database and do not use the forecasts. Figure 5 shows the bias distribution for the ATMS and NAVGEM products (left panel) with the cumulative probability distribution shown in the right panel. The general characteristic of a lower bias and a near equally balanced CPD is expected to provide improved turbulent flux estimations in application to ocean models.

Table 5: ATMS air temperature global performance. The global performance of the algorithms is compared to the atmospheric model performance. Units are degree Centigrade. Comparisons are based on match up data from 01 Jan 2013 through 11 Jan 2014 and contain 116110 observations. The combined results show the 99% CL ranges.

	ME	SD	RMSE	R²
Ascend - Clear	0.157	1.82	1.83	0.966
Ascend - Cloudy	0.036	1.86	1.86	0.966
Descend - Clear	0.127	1.34	1.34	0.978
Descend - Cloudy	0.015	1.66	1.66	0.968
Combined				
ATMS	0.03/0.91	--	1.53/1.76	0.98/0.98
NAVGEM	-0.66/-0.50	--	1.61/1.84	0.98/0.98

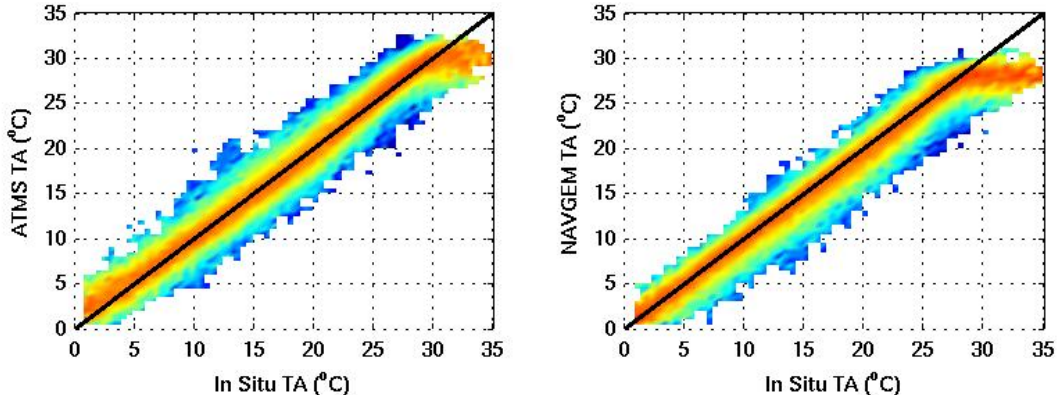


Figure 4: ATMS and NAVGEM TA performance. As in Figure 2, but for TA.

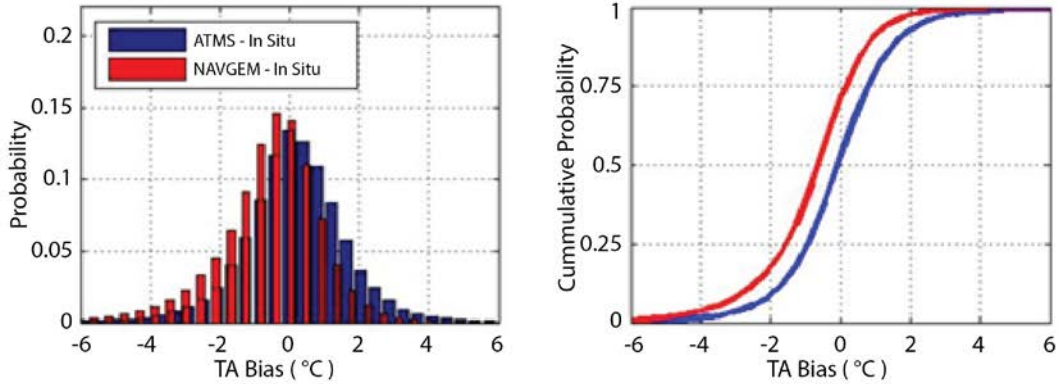


Figure 5: ATMS and NAVGEM TA global bias. As in Figure 3, but for TA.

3. GCOM-Water 1 Advanced Microwave Scanning Radiometer-2 Sensor

The Advanced Microwave Scanning Radiometer-2 (AMSR2) flies aboard the Global Change Observation Mission (GCOM). The first of three water-observing satellites, it is designated GCOM-W1. AMSR2 is a passive microwave sensor with a conical scanner similar to the SSMIS sensor in channel frequency and polarization, as shown in Table 6. The AMSR2 sensor is capable of providing all three surface state variables: TA, QA, and U10. It flies as part of the “A-Train” afternoon constellation (see <http://atrain.nasa.gov/atrainsats.php>) with an ascending node local time of 1330. The polynomial algorithm basis selected was outlined in section 2.1 for the ATMS sensor.

Table 6: GCOMW1 AMSR2 channels. The frequencies and polarizations are similar to those of a DMSP SSMIS sensor.

Frequency(GHz)	6.925/7.3	10.65	18.7	23.8	36.5	89.0
Polarization	Vertical and Horizontal					
IFOV (cross by along-track km)	35x62	24x42	14x22	15x26	7x12	3x5
Swath width (km)	1450 km					

3.1 JAXA Level-1R Data

Previously, Level-1B products were used for all SDR products. The Level-1B product provides a physical temperature in Kelvin for each instantaneous field of view (IFOV) for each sensor channel that has been geo-located on the Earth. However, each channel has a slightly different size, so the area imaged by the satellite is not fully consistent between frequencies. To overcome this issue, JAXA provides a Level-1R product that reweights the IFOVs and averages them into a single resolution. The Level-1R data associated with

the IFOV of the 10.65 GHz channel was selected for NFLUX. This resulted in an SDR dataset of 10.65 to 89.0 GHz channels.

3.2 Rain Flagging of Data

The two AMSR2 rain flags are based on the SSMIS rain flags, which were discussed in section 2.1.1 of Van de Voorde et al. (2014.) The channels used for AMSR2 are similar, but not identical to, those used for SSMIS. Grody (1991) used the lower frequency channels of SSMI to estimate the brightness temperature of the 85 GHz vertically polarized channel. Any scattering due to rain would then impact the lower frequencies more than the higher 85 GHz channel. The AMSR2 database was used to establish the coefficients for a calculated 89V GHz channel using the 18.7 and 23.8 GHz vertically polarized channels with the form of $F=A+B(TB_{18V})+C(TB_{23V})+D(TB_{23V})^2$ following Grody (1991), where TB is the brightness temperature channel. The coefficients were found to be: -85.162, -0.24724, 2.6997, and -0.0041514. Grody (1991) used $SI85=F-TB_{85V}$ to estimate the scattering index (SI) for the 85 GHz channel, with a threshold of $SI85<10K$ to detect scattering from all surfaces. In order to estimate this threshold value for the SI89, the ratio of the vertical to horizontal 36 GHz channel (R36) was used in conjunction with the atmospheric model's daily precipitation values extracted from the match up database. As moisture and precipitation increase, the value of R36 decreases towards unity. Thresholds to identify precipitation were selected at $SI89=7.5K$ and $R36=1.2$. Observations with $SI89$ less than 7.5K and $R36$ greater than 1.2 are assumed to be free of degradation due to precipitation.

3.3 Clear/Cloudy

The method used to estimate the amount of water vapor in the atmosphere and determine whether a particular IFOV is ‘clear’ or ‘cloudy’ is based on Weng and Grody (1994). They presented three equations using the 19(V, vertically-polarized channel) GHz channel to identify when LWP was greater than 0.6 mm, the 37(V) GHz for when it was greater than 0.2 mm, and the 85(V) GHz channel for other conditions. In each case, the 22(V) GHz channel was also utilized. The AMSR2 uses slightly different frequencies than the SSM/I sensor used by Weng and Grody (1994). For the AMSR2 sensor, the 36(V) and 23(V) GHz channels are used. Equation (1) shows the resulting expression:

$$LWP36 = a_0[\ln(290-TB_{36V})-a_1-a_2\ln(290-TB_{23V})], \quad (1)$$

where a_0 was used directly from Weng and Grody (1994) with a value of -1.15, a_1 was estimated to be 2.623 and a_2 to be 0.3949. Similar to the ATMS processing, the Roberts et al. (2010) threshold value of 0.025 mm water was used to distinguish clear and cloudy IFOVs.

3.4 AMSR2 Performance

The performance of the AMSR2 algorithms for all three surface state variables is shown in Figure 6. Figure 7 shows the corresponding plots for NAVGEM. Qualitatively, the trends remain the same: both sources provide very linear match ups to the in situ values; NAVGEM demonstrates a lower degree of scatter; and, NFLUX products demonstrate an improved bias as well as improved performance at the higher ranges of the physical values. The match up period used was from January 2013 to January 2014.

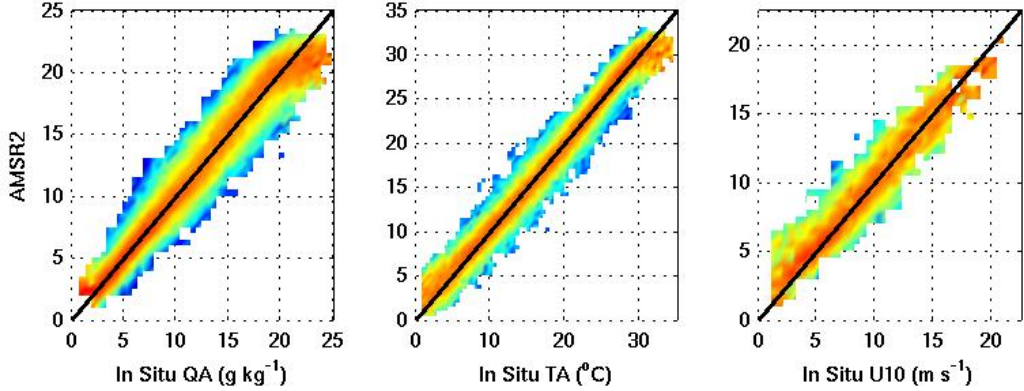


Figure 6: AMSR2 performance. The three observations sets (QA, left; TA, center; and U10, right) are compared to the in situ observations. The U10 uses only buoy observations.

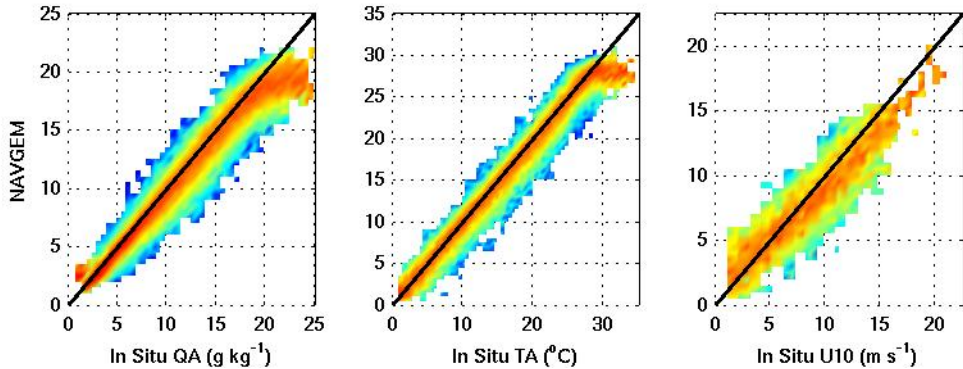


Figure 7: NAVGEM performance. Similar to Figure 6, but for NAVGEM.

Table 7 shows the global performance for each algorithm, while Table 8 shows the overall performance for each variable. Table 8 shows NFLUX AMSR2 products outperform globally the NAVGEM products with respect to ME. The only product where NFLUX AMSR2 RMSE statistically exceeds the NAVGEM RMSE is the wind speed product. The wind speed match up is for buoy-only winds. This represents a change from prior work. Buoy-only winds provide a more controlled match up database that does not rely on large empirical adjustments to account for measurement height and issues of sensor shielding.

Table 7: AMSR2 algorithm performance. The four types of algorithms for each of the surface state parameters are shown. QA units are g kg^{-1} , TA is $^{\circ}\text{C}$, and U10 is in ms^{-1} .

Ascend - Clear	Bias	St Dev	RMSE	R^2
QA	0.180	1.52	1.53	0.959
TA	0.135	1.79	1.79	0.972
U10	0.222	1.14	1.17	0.922
Ascend - Cloudy				
QA	0.167	1.22	1.23	0.974
TA	0.265	1.82	1.84	0.976
U10	0.579	1.87	1.96	0.900
Descend - Clear				
QA	0.124	1.43	1.43	0.962
TA	0.093	1.27	1.27	0.984
U10	0.182	1.32	1.34	0.902
Descend - Cloudy				
QA	0.122	1.15	1.16	0.974
TA	0.142	1.43	1.44	0.983
U10	1.19	2.12	2.43	0.864

Table 8: AMSR2 and NAVGEM performance summary. The combined results for the three products are shown with the associated NAVGEM comparisons. NFLUX products show superior performance for ME. The ranges for a 99% CL level, along with the central value, are shown for the RMSE. The only product that shows a significant difference for the 99% CL is the U10, with NFLUX showing better skill.

AMSR2	ME	SD	RMSE	R^2
QA	0.148	1.37	1.33/1.38/1.43	0.968
TA	0.146	1.57	1.49/1.58/1.68	0.981
U10	0.459	1.62	1.58/1.68/1.79	0.902
NAVGEM				
QA	-0.598	1.26	1.33/1.39/1.45	0.973
TA	-0.544	1.60	1.60/1.69/1.78	0.980
U10	-0.404	2.000	1.96/2.04/2.12	0.838

Figure 8 shows the global PD and CPD for the AMSR2 QA values. Table 9 shows the QA performance for the two peak bands that appear in the global distribution shown in Figure 8. The 99% CL for RMSE are included. The $5\text{-}10 \text{ g kg}^{-1}$ band accounts for 33.6% of the global distribution. The $17\text{ to }22 \text{ g kg}^{-1}$ band accounts for 23.6% of the global distribution. The trend of a higher negative bias, but lower scatter in the data is

maintained in this band for the NAVGEM compared to NFLUX. The 99% CL range for the RMSE indicates for both peak areas in the global distribution, there is no significant difference.

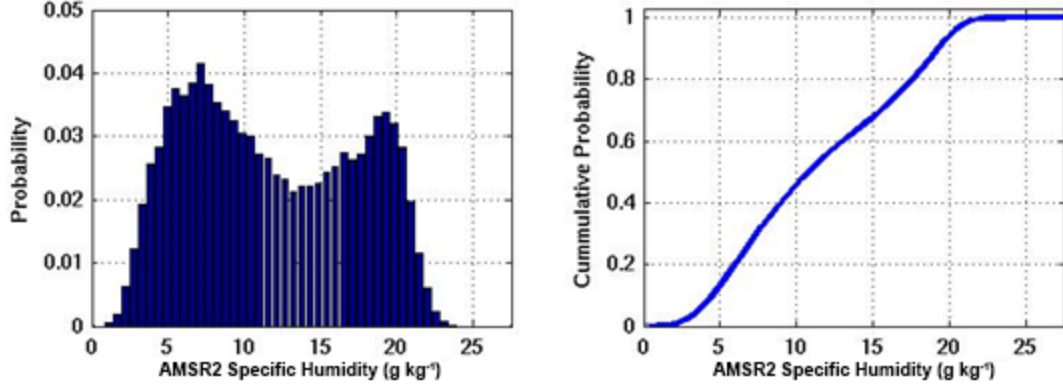


Figure 8: AMSR2 QA global value probability. The panel on the left shows the probability density function of the in situ values for the match up period, with the panel on the right showing the cumulative density function calculated from the data. The 5 to 10 g kg⁻¹, band contains 33.6% of the global distribution and the 17 to 22 g kg⁻¹ band contains 23.6% of the distribution.

Table 9: Match up metrics for QA bands. Comparisons at the 99% confidence levels are shown. The limits were bootstrapped using 5000 random samples of the match up database. At the 99% CL there is no statistical difference in the RMSE error. There does remain a significant improvement in ME for the AMSR2 QA product.

5<QA<10	ME	RMSE	R ²
AMSR2	0.050	1.06/1.04/1.15	0.780
NAVGEM	-0.517	1.13/1.19/1.25	0.823
17<QA<22			
AMSR2	0.484	1.50/1.55/1.59	0.545
NAVGEM	-0.776	1.56/1.61/1.67	0.518

As shown in Figures 6 and 7, center panels, both NFLUX and NAVGEM provide an excellent product throughout the majority of the range of surface air temperature values. Figure 9 shows a different presentation than in the match ups shown in Figures 6 and 7. Here the biases are shown as a function of the in situ TA and the bin colors are not equally weighted as was done in Figures 6 and 7, where the distribution for each bin was normalized. This allows a better visualization of the performance in each region of the distribution of the in situ data. In Figure 9 the bins are weighted/colored based on their actual count, so this represents a two-dimensional probability where warmer colors indicate a higher probability of occurrence.

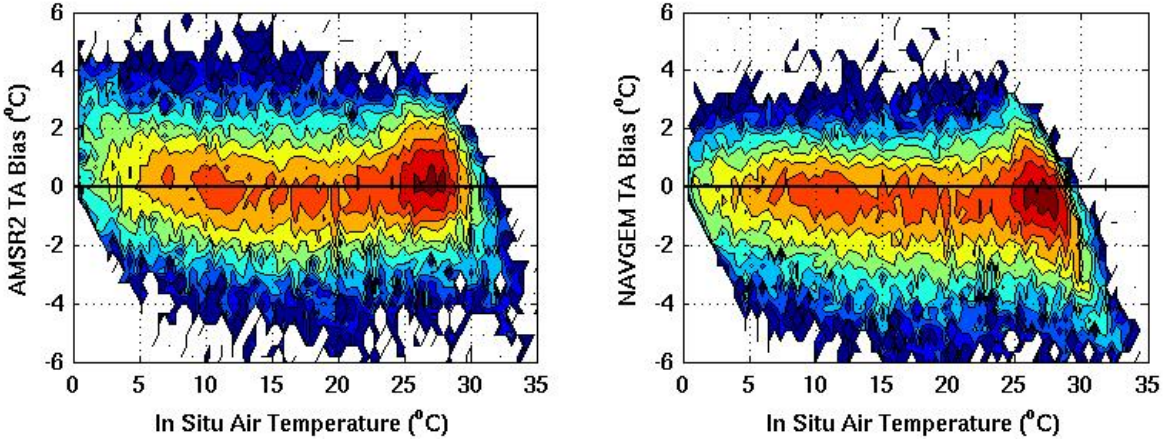


Figure 9: Two-dimensional probability distribution of air temperature bias. Bins have not been normalized and reflect the distribution throughout the range of temperatures. Warm colors indicate a higher density of data and hence a higher probability than cooler colors.

Figure 10 shows the global PD and CPD for the satellite TA values. Thirty-one percent of the observations of air temperature occur when TA is greater than 25 °C. The inflection point within the CPD curve at 25 °C is evident. Sensible heat flux is directly proportional to the difference between the sea surface temperature and the air temperature. In regions where TA exceeds 25 °C, it is possible that NAVGEM TA could overestimate the flux due to a higher temperature gradient, if U10 and the sea surface temperature are correctly forecast. Table 10 shows the NFLUX AMSR2 and NAVGEM statistics for this high TA region. At the 99% CL, the statistics of ME, RMSE, and R^2 are all statistically different between the two data sets. The range for the RMSE is shown, as AMSR2 high TA is 1.39 to 1.66 °C, while the NAVGEM has a range of 1.72 to 1.96 °C.

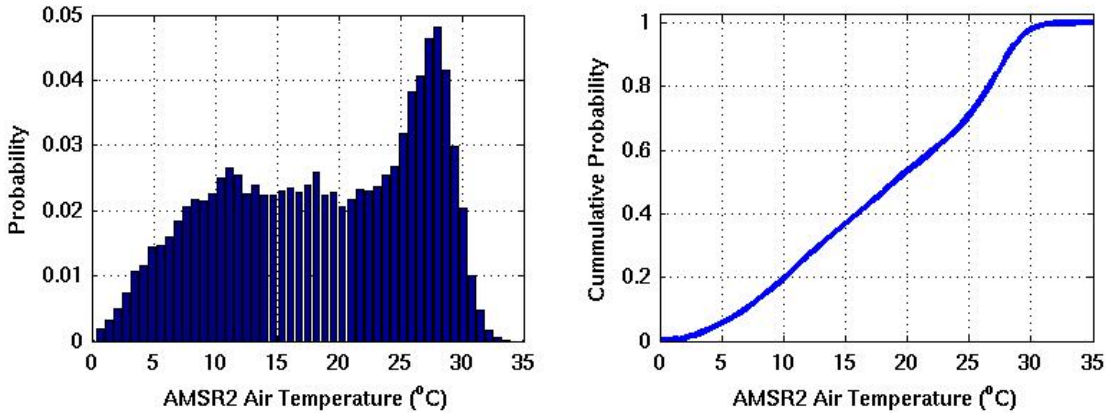


Figure 10: AMSR2 TA global value probability. Similar to Figure 8, but for TA. Air temperatures greater than 25 °C account for 31% of the global matched up data.

Table 10: Match up metrics for TA high values. The RMSE values indicate the range and value at a 99% CL. The values are shown in $^{\circ}\text{C}$.

25<TA	ME	RMSE	R^2
AMSR2	0.153	1.39/1.52/1.66	0.640
NAVGEM	-0.778	1.72/1.82/1.96	0.478

The wind speed global performance shown in Table 8 indicates that the performance of the NFLUX and NAVGEM products are similar. One exception is that the NFLUX wind speed RMSE is better at the 99% CL than NAVGEM. Examination of the match up normalized distributions shown in the right panels of Figures 6 and 7 indicate that at higher wind speeds, the NAVGEM products are under-predicting the true wind speed. The core of the distribution peak, with reference to the black line, indicates that NAVGEM under predicts wind speed by an increasing amount as the in situ value increases.

Figure 11 shows a two-dimensional PDF for the global wind speed bias. Figure 7, right panel, shows that at an in situ value of 10 ms^{-1} , the mean NAVGEM value is $9.0 \pm 2.2 \text{ ms}^{-1}$. The NFLUX value is $10.4 \pm 2.3 \text{ ms}^{-1}$, from Figure 6, right panel. A subset of all wind speeds greater than 10 ms^{-1} , shown in Table 11, accounts for 25.2% of the data set. The mean bias and RMSE for this band of match ups show significant improvement using AMSR2 observations at the 99% CL.

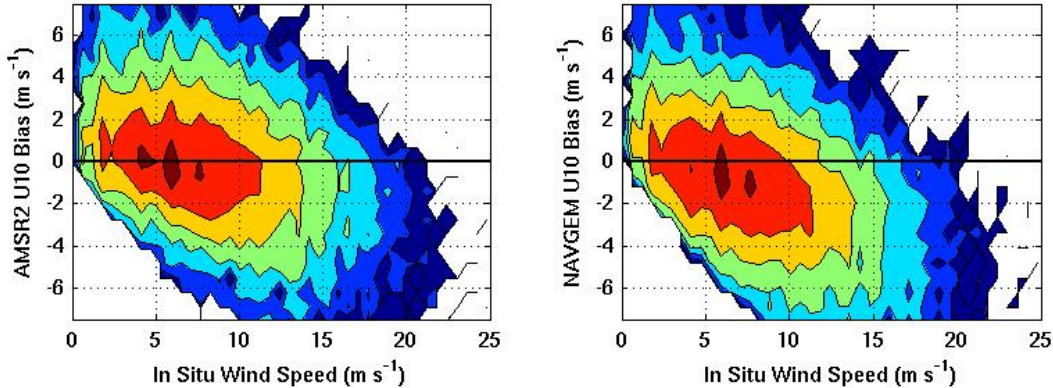


Figure 11: Two-dimensional probability distribution of wind speed bias. Similar to Figure 9, but for U10. The distribution of the U10 bias for both the AMSR2 and NAVGEM products are shown as a function of the in situ buoy-only U10. Warmer colors show higher probabilities.

Table 11: Performance metrics for wind speeds greater than 10 ms^{-1} . This accounts for 25.2% of all measured wind speeds during the match up period. The differences between the ME and RMSE are statistically significant at the 99% CL level. The correlation coefficients (R^2) are statistically equal. The values are shown in ms^{-1} .

10<U10	ME	RMSE	R^2
AMSR2	-0.860	2.84/2.95/3.06	0.520
NAVGEM	-2.27	3.60/3.69/3.78	0.482

The match up distributions for wind speeds above and below 10 ms^{-1} is shown in Figures 12 and 13. The blue dots indicate the mode of the distribution in each 0.5 ms^{-1} bin. The difference between the two products is significant, with the AMSR2 U10 product indicating better agreement with the in situ measurements than the NAVGEM product.

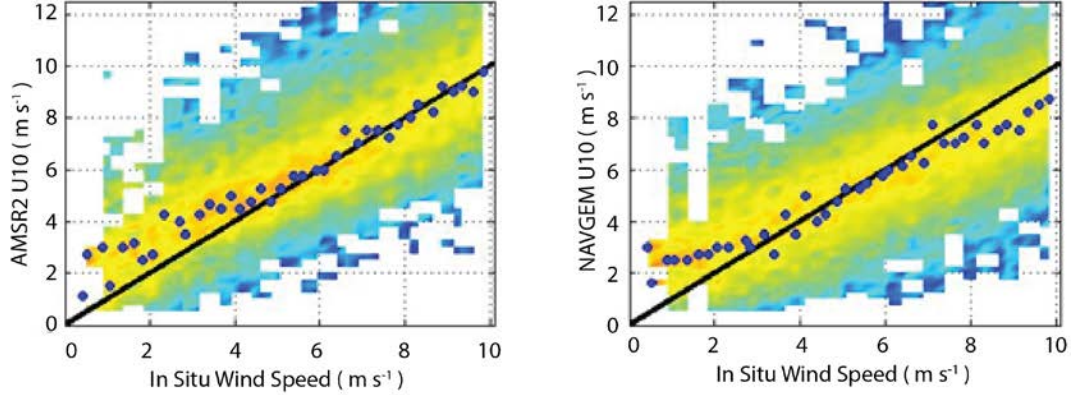


Figure 12: Probability distribution of lower wind speeds as a function of the in situ wind speed. AMSR2 and NAVGEM are compared. Blue dots indicate the mode of the distribution of the in situ 0.5 ms^{-1} bins. AMSR2 shows a high bias below roughly 4 ms^{-1} . NAVGEM shows a high bias below 3 ms^{-1} but a low bias above 7.5 ms^{-1} that is not evident in the AMSR2 distribution.

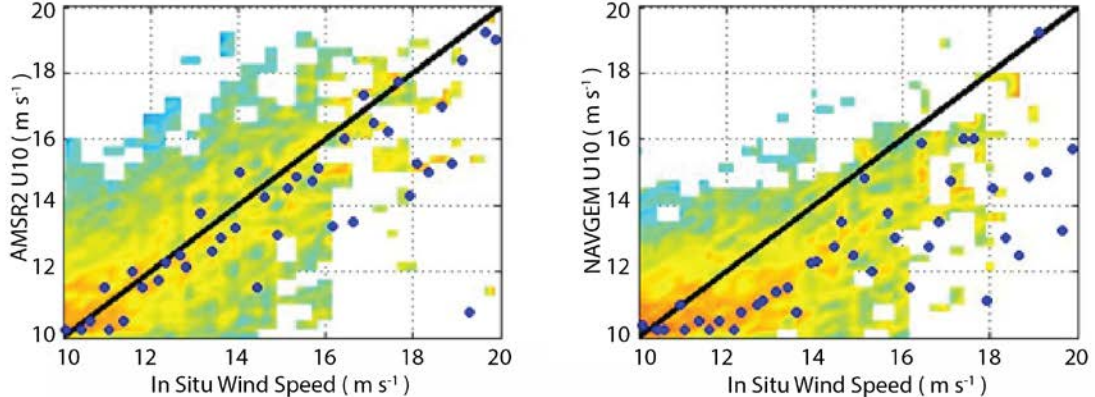


Figure 13: Probability distribution for higher wind speeds. Similar to Figure 12. The low bias for the NAVGEM product noted in the lower wind speeds is highly evident. AMSR2 shows a scattered lower bias beginning around 15 ms^{-1} .

4. SSMIS Update

AMSR2 is similar to the SSMIS sensor, with AMSR2 demonstrating skill in measuring air temperature. This provided a rationale to reexamine the SSMIS algorithms. The products for SSMIS have been expanded to include TA, in addition to QA and U10. Also supporting a reexamination was a 1 K bias between the ascending and descending node brightness temperatures noted by Sapiano and Berg (2013) while working on an intercalibration project for the F16, F17, and F18 SSMIS sensors. The algorithms were

redeveloped using the new polynomial regression approach, with separate algorithms for ascending/descending swaths under clear/cloudy conditions.

4.1 Rain Flagging and Clear/Cloudy SSMIS

The rain flagging of the data was discussed in section 2.1.1 of Van de Voorde et al. (2014). The SSMIS reader code still uses Equations 1 and 2 of that report. The clear/cloudy calculation utilizes Equation 10 of Weng and Grody (1994) with updated coefficients for the 37(V) and 22(V) GHz channels. The LWP estimation used in the updated SSMIS system is

$$LWP_{37} = -1.15 \times [\ln(290-TB_{37V}) - 2.7603 - 0.3716 \times \ln(290-TB_{22V})] \quad (2)$$

The same threshold of 0.025 mm water for the clear/cloudy determination is used.

4.2 SSMIS Performance

The new air temperature product performance is shown in Table 12. This is contrasted with the ATMS and AMSR2 TA data shown in Table 5 and Table 7, respectively, and the summary AMSU TA data shown in Table 4. The range of the RMSE data for other TA products is 1.27 °C (for the AMSR2 descending clear type) to 1.86 °C (for ATMS ascending cloudy type). The DMSP/SSMIS satellites show an RMSE range of 1.50 to 1.87 °C. There are no prior SSMIS TA results to compare with; these are within the range of the current products.

Table 12: SSMIS air temperature algorithm performance. The individual performance of each of the four algorithm types for each SSMIS is shown. The clear/cloudy determination uses a liquid water path threshold of 0.025 mm. All values are shown in °C with the exception of the correlation coefficient (R^2).

F16	ME	SD	RMSE	R²
Ascend – Clear	0.024	1.83	1.83	0.971
Ascend – Cloudy	0.104	1.86	1.87	0.968
Descend - Clear	0.127	1.50	1.51	0.979
Descend - Cloudy	0.131	1.66	1.67	0.976
F17				
Ascend - Clear	0.093	1.79	1.80	0.974
Ascend - Cloudy	0.214	1.86	1.87	0.967
Descend - Clear	0.084	1.49	1.50	0.980
Descend - Cloudy	0.066	1.62	1.62	0.980
F18				
Ascend - Clear	0.114	1.55	1.56	0.979
Ascend - Cloudy	0.160	1.75	1.76	0.973
Descend - Clear	0.130	1.74	1.75	0.974
Descend - Cloudy	0.166	1.80	1.80	0.974

The updated performance of the SSMIS QA product is shown in Table 13. Table 4 shows the previous combined F16, F17, and F18 QA performance with an RMSE of 2.049 g kg⁻¹. The overall performance of the newer algorithms shows improvement, with a high RMSE of 1.86 g kg⁻¹ for the F18 descending clear QA algorithm, and a low of 1.22 g kg⁻¹ water for the F17 ascending cloudy QA algorithm. For comparison, AMSR2 is a very similar sensor, and the lowest RMSE value is 1.16 g kg⁻¹ using the descending cloudy condition, from Table 7.

Table 13: SSMIS specific humidity algorithm performance. Similar to Table 12. All values are shown in g kg⁻¹ with the exception of the correlation coefficient (R²).

F16	ME	SD	RMSE	R²
Ascend - Clear	0.534	1.73	1.81	0.951
Ascend - Cloudy	0.220	1.25	1.27	0.965
Descend - Clear	0.321	1.62	1.65	0.955
Descend - Cloudy	0.239	1.25	1.27	0.967
F17				
Ascend - Clear	0.475	1.74	1.81	0.952
Ascend - Cloudy	0.242	1.20	1.22	0.966
Descend - Clear	0.435	1.63	1.69	0.957
Descend - Cloudy	0.126	1.23	1.24	0.971
F18				
Ascend - Clear	0.525	1.72	1.79	0.954
Ascend - Cloudy	0.185	1.23	1.24	0.969
Descend - Clear	0.655	1.74	1.86	0.956
Descend - Cloudy	0.240	1.28	1.30	0.971

The updated performance of the SSMIS U10 product is shown in Table 14. The performance for SSMIS wind speed indicates marked improvement, especially under clear conditions. The bias and standard deviation have both been reduced. The correlation coefficient is, with one exception, greater than 0.8. The previously developed SSMIS algorithm combined performance is shown in Table 4. The updated RMSE for the clear atmospheric conditions is reduced by more than 1 ms⁻¹.

Table 14: SSMIS wind speed algorithm performance. Similar to Table 12. Data matchup is to buoy-measured wind speeds. All values are shown in ms^{-1} with the exception of the correlation coefficient (R^2).

F16	ME	SD	RMSE	R²
Ascend - Clear	0.221	1.43	1.45	0.864
Ascend - Cloudy	-0.286	2.50	2.52	0.837
Descend - Clear	0.111	1.47	1.47	0.871
Descend - Cloudy	-0.084	2.55	2.55	0.825
F17				
Ascend - Clear	0.388	1.45	1.50	0.826
Ascend - Cloudy	0.073	2.49	2.49	0.839
Descend - Clear	0.321	1.62	1.65	0.860
Descend - Cloudy	0.012	2.85	2.85	0.780
F18				
Ascend - Clear	0.419	1.41	1.47	0.818
Ascend - Cloudy	-0.141	2.49	2.49	0.816
Descend - Clear	0.286	1.56	1.59	0.871
Descend - Cloudy	-0.139	2.68	2.69	0.811
All				
	0.228	1.79	1.81	0.867

Table 15 shows the overall comparison of each SSMIS sensor and the combined performance for each product. Table 4 shows the prior performance of SSMIS QA and U10. The new QA performance shows reduction in RMSE of 0.32 to 0.42 g kg^{-1} (using the median values) from the original SSMIS QA value of 2.05 g kg^{-1} , and an increase in correlation coefficient of 0.1. The newer atmospheric model, NAVGEM, also shows remarkable improvement compared to the previous atmospheric model, the Navy Operational Global Atmospheric Prediction System (NOGAPS). Where NOGAPS had an RMSE of 1.94 g kg^{-1} in the match up data from Table 5 in Van de Voorde et al. (2014) (using 2010-2011 data), NAVGEM RMSE is reduced to 1.39 g kg^{-1} (using 2013 data). The 99% CL show that the global NAVGEM QA is better than SSMIS QA by at least 0.13 g kg^{-1} . The SSMIS U10 also shows substantial improvement. Previously the overall RMSE for U10 was 2.83 ms^{-1} . The new values show a range of 1.74 to 1.83 ms^{-1} (using the median values in Table 15). This is a reduction of 1 ms^{-1} in the errors. Correlation coefficients have also improved, from 0.43 to 0.87.

Table 15: SSMIS and NAVGEM performance summary. Only NAVGEM QA performance is statistically better at the 99% confidence limit than the three SSMIS products. The low, mid, and high range for the NAVGEM QA is shown. Air temperature RMSEs are indistinguishable at the 99% CL. The NFLUX wind speed is superior. The wind speed match ups use only buoy-measured wind speeds.

QA (g kg^{-1})	ME	RMSE	R^2
F16	0.375	157/1.63/1.68	0.960
F17	0.387	1.58/1.63/1.69	0.962
F18	0.516	1.68/1.73/1.79	0.961
NAVGEM	-0.561	1.34/1.39/1.44	0.973
TA ($^{\circ}\text{C}$)			
F16	0.086	1.62/1.70/1.77	0.977
F17	0.098	1.57/1.66/1.77	0.979
F18	0.130	1.60/1.69/1.78	0.978
NAVGEM	-0.434	1.51/1.59/1.67	0.983
U10 (ms^{-1})			
F16	0.097	1.66/1.74/1.83	0.870
F17	0.282	1.74/1.83/1.93	0.866
F18	0.255	1.68/1.77/1.86	0.873
NAVGEM	-0.439	2.22/2.30/2.39	0.785

The NFLUX SSMIS products compared to NAVGEM show comparable performance. In all cases the SSMIS bias or mean error is closer to zero at the 99% CL level than is the NAVGEM mean error. The NAVGEM QA product outperforms the SSMIS QA product with respect to the RMSE 99% CL limits. There is no statistical difference between the RMSEs for TA. At all levels the SSMIS U10 product offers superior data performance when compared with the NAVGEM U10 data.

5. AMSU Update

In a similar approach to that for SSMIS, the entire set of AMSU algorithms was updated from a simple multiple linear regression for each satellite/product pair to distinct multiple polynomial regressions for ascending/descending swath directions as well as clear/cloudy atmospheric conditions. The clear/cloudy determination is the same as that used for ATMS, discussed in section 2.3. The performance metrics of the POES/AMSU (Metop/AMSU) sensors are shown in Table 16 (Table 17).

Table 16: POES AMSU algorithm performance. The performance for each of the satellite and their associated matrix of algorithms for ascending/descending and clear/cloudy conditions are shown for the two products produced by the AMSU sensor.

N15	Prod	ME	SD	RMSE	R²
Ascend - Clear	QA	0.184	1.54	1.55	0.946
	TA	0.048	1.37	1.37	0.972
Ascend - Cloudy	QA	-0.327	1.80	1.83	0.931
	TA	-0.631	2.55	2.63	0.916
Descend - Clear	QA	0.179	1.58	1.59	0.947
	TA	0.188	1.75	1.76	0.961
Descend - Cloudy	QA	-0.387	1.80	1.84	0.912
	TA	-0.334	2.40	2.42	0.923
N18					
Ascend - Clear	QA	0.144	1.52	1.53	0.948
	TA	0.009	1.34	1.34	0.974
Ascend - Cloudy	QA	-0.192	2.11	2.12	0.915
	TA	-0.204	2.33	2.34	0.931
Descend - Clear	QA	0.247	1.56	1.58	0.949
	TA	0.034	1.82	1.82	0.960
Descend - Cloudy	QA	-0.110	2.33	2.33	0.914
	TA	-0.824	2.65	2.77	0.919
N19					
Ascend - Clear	QA	0.060	1.46	1.47	0.951
	TA	-0.062	1.28	1.28	0.977
Ascend - Cloudy	QA	-0.962	1.66	1.92	0.917
	TA	-0.849	2.45	2.59	0.929
Descend - Clear	QA	0.193	1.61	1.63	0.946
	TA	0.044	1.82	1.82	0.960
Descend - Cloudy	QA	-0.157	2.24	2.25	0.922
	TA	-1.12	2.97	3.17	0.909

Table 17: Metop AMSU algorithm performance. Similar to Table 16 for the AMSU sensors onboard the Metop satellites.

Metop 1	Prod	ME	SD	RMSE	R ²
Ascend - Clear	QA	0.149	1.62	1.63	0.946
	TA	0.100	1.66	1.67	0.962
Ascend - Cloudy	QA	-0.072	2.26	2.26	0.920
	TA	-0.122	2.54	2.54	0.944
Descend - Clear	QA	0.112	1.52	1.53	0.946
	TA	0.0102	1.37	1.37	0.971
Descend - Cloudy	QA	-0.155	1.82	1.83	0.921
	TA	-0.357	2.24	2.27	0.943
Metop 2					
Ascend - Clear	QA	0.147	1.60	1.61	0.945
	TA	0.164	1.74	1.74	0.958
Ascend - Cloudy	QA	-0.318	2.28	2.30	0.922
	TA	-0.117	2.85	2.85	0.931
Descend - Clear	QA	0.155	1.57	1.58	0.943
	TA	0.095	1.42	1.42	0.969
Descend - Cloudy	QA	-0.523	1.76	1.83	0.920
	TA	-0.568	1.85	1.94	0.958

5.1 AMSU Performance

Examination of the errors associated with each of the algorithm types (e.g. Ascending/Clear, Descending/Cloudy) in Tables 16 and 17 indicate that for the QA product, the ‘clear’ conditions are superior to the cloudy conditions. Additionally for the POES AMSUs the ascending direction provides the lowest RMSE values. In the case of the Metop AMSUs the lowest RMSE is on the descending orbits. This is presumably due to the different conditions the sensors are viewing on the ascending orbits. Table 1 shows the POES spacecraft are ascending in the mid- to late-afternoon, while the Metop are in the evening. It is assumed then that the diurnal effect is a factor in these results. This pattern is also noted in the TA products.

Table 18 shows the combined summary statistics for the AMSU sensors compared to the matched up NAVGEM model observations. The range and mode of the RMSE errors using a 99% CL are shown with the Table. These newer results compare very similarly to those shown in Table 4 for the older multiple linear regression algorithms. NAVGEM provides a better product than the NFLUX AMSU QA products at this confidence level. For the TA product, there is no statistical difference between the two sources with the exception of the TA product from N19. The lower limit on the NFLUX AMSU RSME is 1.79 °C, while the upper limit for the NAVGEM TA is 1.72 °C.

Table 18: AMSU and NAVGEM performance summary. The resultant statistics when all four algorithms are combined into a single performance set. The matched up NAVGEM data is also shown.

N15	ME	SD	RSME	R²
QA	0.040	1.64	1.56/1.64/1.73	0.959
TA	-0.034	1.86	1.72/1.86/2.01	0.973
N18				
QA	0.108	1.74	1.63/1.74/1.89	0.954
TA	-0.106	1.87	1.72/1.87/2.04	0.972
N19				
QA	-0.043	1.69	1.60/1.69/1.79	0.955
TA	-0.234	1.94	1.79/1.95/2.12	0.970
Metop 1				
QA	0.078	1.69	1.59/1.69/1.80	0.956
TA	-0.009	1.75	1.64/1.75/1.86	0.975
Metop 2				
QA	0.023	1.70	1.61/1.70/1.79	0.956
TA	0.018	1.77	1.66/1.77/1.88	0.975
NAVGEM				
QA	-0.629	1.31	1.39/1.45/1.51	0.971
TA	-0.518	1.56	1.57/1.64/1.72	0.980

6. Summary and Discussion

The NFLUX system now includes twelve separate satellites, four of which provide wind speed, air temperature, and specific humidity via a single platform. The combined number of orbits provided by the system is approximately 168 per day. The inclusion of the two new satellites (SNPP/ATMS and GCOM-W1/AMSR2) further enhances the global coverage, and these two new sensors provide wider swaths than either the AMSU or SSMIS sensors.

The performance of the new algorithms in general shows improvement over the prior algorithms as shown in Table 19. The bias shows a decrease with the exception of the SSMIS QA, which nevertheless shows a significant decrease in the RMSE. The AMSU QA and TA RMSE show increases, but at the 99% CL (not shown here) there is no difference between these two values. As discussed in section 3.4, buoy-only measurements were used for wind speed algorithm development and subsequent match

ups. The buoy-only database provided a higher degree of quality control than using both buoy and commercial vessel observations.

Table 19: Comparison of older algorithm performance with newer algorithms. The new algorithms provide unique coefficients for the ascending/descending-clear/cloudy matrix.

Sensor/Product	ME	RMSE	R ²	Notes
AMSU QA Old	-0.331	1.62	0.91	g kg ⁻¹ water
AMSU QA New	0.041	1.69	0.91	
ATMS QA	0.15	1.48	0.93	
AMSU TA Old	-0.25	1.66	0.96	°C
AMSU TA New	-0.07	1.84	0.95	
ATMS TA	0.12	1.64	0.96	
SSMIS QA Old	-0.22	2.05	0.86	g kg ⁻¹ water
SSMIS QA New	0.433	1.67	0.92	
AMSR2 QA	0.15	1.38	0.94	
SSMI U10 Old	0.62	2.83	0.43	ms ⁻¹
SSMI U10 New	0.23	1.81	0.87	Buoy only match up
AMSR2 U10	0.46	1.68	0.81	Buoy only match up

The goals of the NFLUX development include improvement in the estimation of heat fluxes into and out of the ocean surface, and as a consequence improvement in the forecasts of the upper ocean environment. The NFLUX_PRE system focused on the development of improved surface state variables used in the bulk formulas for latent and sensible turbulent heat fluxes.

Persistent biases in the surface heat fluxes alter the evolution of the upper ocean in forecast systems, but it is difficult to estimate the combined impact of persistent biases in the surface ocean state variable fields of TA, QA, and U10. The bulk coefficients of exchange used to estimate the turbulent fluxes are functions of the wind speed (Liu et al., 1979.) Figure 14 shows the mode of the distributions of the NFLUX wind speed (blue) from all sources and NAVGEM wind speeds (green) compared to the buoy-measured wind speeds. The 90% confidence limits are also shown for 2.5, 5, 10, and 15 ms⁻¹ wind speeds. The left panel reinforces the characterization that NAVGEM is likely to underestimate the wind speed throughout the entire range of winds. Liu et al. (1979) show the exchange coefficients peak at approximately 5 ms⁻¹, then decline. Therefore, it is difficult to assess the impact of a global bias in NAVGEM wind speed or the results of applying a uniform bias correction. Follow-on work comparing the impact on ocean models of using the NFLUX retrievals of TA, QA, and U10 blended with NAVGEM forecasts will address this question.

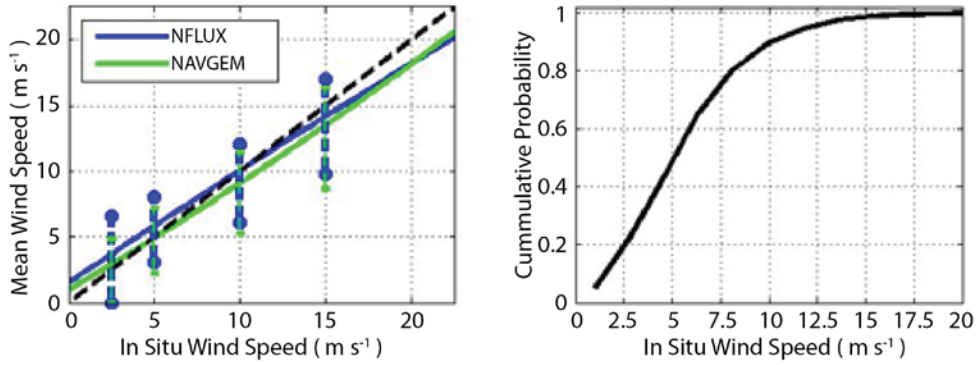


Figure 14: Mean wind speed compared to buoy winds. The modes of the wind speed distributions for NFLUX and NAVGEM compared to the in situ buoy winds are shown in the left panel. The vertical lines indicate the 90% confidence limits based on the actual match up data. The dashed line shows a 1:1 correlation with the buoy winds. The right panel shows the distribution of global wind speeds greater than 0.5 ms^{-1} .

7. References

Grody, N.C. (1991). Classification of Snow Cover and precipitation Using the Special Sensor Microwave Imager. *J. Geophys. Res.*, **96**, D4, 7423-7435.

Grody, N., J. Zhao, R. Ferraro, F. Weng, and R. Boers (2001). Determination of perceptible water and cloud liquid water over oceans from the NOAA 15 advanced microwave sounding unit. *J. Geophys. Res.*, **106**, 2943-2953.

Hu, J-C., W-J. Chen, C-C. Li, C-C. Chao (2006). Rainfall Estimation of Mesoscale Convective Systems using AMSU-A data during the Mei-Yu Season. *Terr. Atmos. Ocean. Sci.*, **17**, 91-109.

John, V.O., R.P. Allan, W. Bell, S.A. Buehler, and A. Kottayil (2013). Assessment of intercalibration methods for satellite microwave humidity sounders. *J. Geophys. Res.*, **118**, 10, 4906-4918.

Liu, W.T., K.B. Kataros, J.A. Businger (1979). Bulk Parameterization of Air-Sea Exchanges of Heat and Water Vapor Including the Molecular Constraints at the Interface. *J. Atmos. Sci.*, **26**, 1722-2802.

Roberts, J.B., C.A. Clayson, C.A., F.R. Robertson, and D.L. Jackson (2010). Predicting near-surface atmospheric variables from Special Sensor Microwave/Imager using neural networks with a first-guess approach. *J. Geophys. Res.*, **115**, D19, doi: 10.1029/2009JD013099.

Sapiro, M. R. P. and W. Berg (2013). *Intercalibration of SSM/I and SSMIS for the CSU FCDR*. Technical Report. Colorado State University. Obtained from <http://rain.atmos.colostate.edu/FCDR>.

Van de Voorde, N.E., J. May, and C. Rowley (2014). *Validation Test Report for NFLUX PRE: Validation of Specific Humidity, Surface Air Temperature, and Wind speed Precision and Accuracy for Assimilation into Global and Regional Models*. NRL Memorandum Report NRL/MR/7320-14-9523. Naval Research Laboratory, Oceanography Division, Stennis Space Center, MS 39529.

Weng, F.Z. and N.C. Grody (1994). Retrieval of Cloud Liquid Water Using the Special Sensor Microwave Imager (SSM/I). *J. Geophys. Res.*, **99**, D12, 25535—25551.

Weng, F., X. Zou, X. Wang, S. Yang, and M.D. Goldberg (2012). Introduction to Suomi national polar-orbiting partnership advanced technology microwave sounder for numerical weather prediction and tropical cyclone applications. *J. Geophys. Res.*, **117**, D19112, doi:10.1029/2012JD018144.

8. Acronyms and Abbreviations

AMSR-2	Advanced Microwave Scanning Radiometer-2
AMSU	Advanced Microwave Sounding Unit
ATMS	Advanced Technology Microwave Sounder
CL	Confidence Limit
CPD	Cumulative probability distribution
DMSP	Defense Meteorological Satellite Program
EDR	Environmental Data Record
GCOM-W1	Global Change Observation Mission-W1
IFOV	Instantaneous field of view
JAXA	Japanese Aerospace Exploration Agency
LWP	Cloud liquid water path
ME	Mean error (bias)
NAVGEM	Navy Global Environmental Model
NFLUX	Naval Research Laboratory Ocean Surface Flux
NOGAPS	Navy Operational Global Atmospheric Prediction System
PD	Probability distribution
POES	Polar-orbiting Environmental Satellites
QA	Specific humidity
R ²	Correlation coefficient
RMSE	Root-mean square error
SD	Standard Deviation
SDR	Sensor Data Record
SI	Scattering Index
SNPP	Suomi National Polar-orbiting Partnership
SSMIS	Special Sensor Microwave Imager/Sounder
TA	Air temperature
TB	Brightness temperature
U10	Scalar wind speed at 10 meter height
VTR	Validation Test Report

